WAVES IN RANDOM NEURAL MEDIA

S Coombes and H Schmidt
School of Mathematical Sciences
University of Nottingham
Nottingham, NG7 2RD, UK

C R Laing
Institute of Information and Mathematical Sciences
Massey University
Private Bag 102-904, North Shore Mail Centre, Auckland, New Zealand

N Svanstedt
Mathematical Sciences
Chalmers University of Technology and University of Gothenburg
S-412 96 Göteborg, Sweden

J A Wyller
Department of Mathematical Sciences and Technology
Norwegian University of Life Sciences
P. O. Box 5003, NO-1432 As, Norway

Abstract. Translationally invariant integro-differential equations are a common choice of model in neuroscience for describing the coarse-grained dynamics of cortical tissue. Here we analyse the propagation of travelling wavefronts in models of neural media that incorporate some form of modulation or randomness such that translational invariance is broken. We begin with a study of neural architectures in which there is a periodic modulation of the neuronal connections. Recent techniques from two-scale convergence analysis are used to construct a homogenized model in the limit that the spatial modulation is rapid compared with the scale of the long range connections. For the special case that the neuronal firing rate is a Heaviside we calculate the speed of a travelling homogenized front exactly and find how the wave speed changes as a function of the amplitude of the modulation. For this special case we further show how to obtain more accurate results about wave speed and the conditions for propagation failure by using an interface dynamics approach that circumvents the requirement of fast modulation. Next we turn our attention to forms of disorder that arise via the variation of firing rate properties across the tissue. To model this we draw parameters of the firing rate function from a distribution with prescribed spatial correlations and analyse the corresponding fluctuations in the wave speed. Finally we consider generalisations of the model to incorporate adaptation and stochastic forcing and show how recent numerical techniques developed for stochastic partial differential equations can be used to determine the wave speed by minimising the L^2 norm of a travelling disordered activity profile against a fixed test function.

can side-step the use of homogenization theory and develop an alternative perturbative analysis which tracks the position of the wave interface with a greater degree of accuracy. Numerical simulations are presented to highlight both the regime of validity of the homogenization calculations and the improved performance of the interface approach where they break down. We break translation invariance again in section 4, though this time by treating the ring threshold as a random variable. A theory that relates uctuations in the threshold to uctuations in wave speed is developed and shown to be in excellent agreement with numerical simulations. In this section we also treat the case of noise driven neural elds (generalised now to include adaptation) and develop a numerical technique for the determination of wave speed based on recent *freezing* techniques developed for the study of stochastic partial di erential equations. Finally in section 5 we discuss further challenges for the study of waves in random neural media.

2. **Homogenization for periodically modulated connectivities.** To incorporate the known microstructure of visual cortex within a large-scale modelling framework Bresslo has proposed the use of periodically modulated connectivity kernels [9

where

$$w\ (x;y) =\quad 1$$

Figure 1. Simulations of (1)-(6) for (top to bottom) $\epsilon = 0$, 0.1, 0.5 and 0.9. $u(x; t)$ is shown color-coded. Other parameters are $h = 0.3$, $\beta = 20$ and $\tau = 5$.

Since $\phi(y) = 1 + \epsilon \sin(2\pi y)$ it is natural to perform a change of variable, $z = e^{2\pi iy}$, so that we may rewrite (11) in the form of a contour integral around the unit circle in the complex plane as

$$\mathcal{I} = \frac{c}{2\pi} \oint \frac{dz}{(z - z_+)(z - z_-)}; \qquad \mu = h - 1 = 2; \tag{12}$$

where

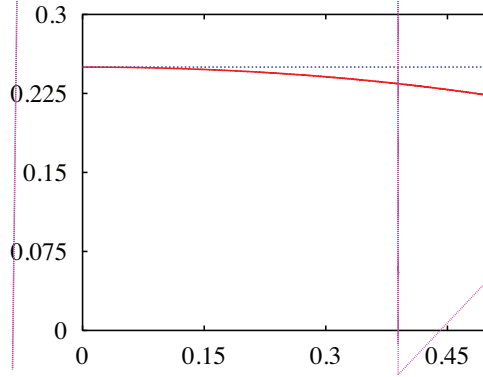$$z_\pm = -(1 + c)i \pm i\sqrt{(1 + c)^2 - \epsilon^2}: \tag{13}$$

Figure 2. A plot of $c = c(\epsilon)$ for the case of a travelling front calculated for a Heaviside firing rate with threshold $h = 0.4$ in the homogenized model (solid line, red). Also shown are simulation results for $\gamma = 2$ (crosses, red) as well as a theoretical curve (dotted line, magenta) obtained from an interface dynamics calculation.

For small ϵ the only pole in the unit circle is z_+ and we may use the calculus of residues to show that

$$\beta = \frac{1}{2} - \gamma \frac{c}{(1+c)^2 - \epsilon^2} ; \qquad (14)$$

Solving (14) for c gives

$$c = 2\gamma \left(\frac{-2\beta + \sqrt{1 + \epsilon^2(4\beta^2 - 1)}}{4\beta^2 - 1} \right) ; \qquad (15)$$

A plot of $c = c(\epsilon)$ is shown in Fig. 2. Corresponding wave profiles from (9) are shown in Fig. 3. In the limit $\epsilon \to 0$ we recover the result for the homogeneous model (no modulation):

$$c = \frac{1 - 2h}{2h} ; \qquad (16)$$

As expected there is good agreement between the analysis of the homogenized model and simulations of the full model only for small ϵ. Also shown in this figure is another theoretical curve, with better agreement over a larger range of ϵ. The derivation of this curve side-steps the need for homogenization theory, though is only valid in the special case that $f(u) = H(u - h)$. We explain this result next.

3. **Beyond homogenization.** Following ideas recently developed in [11] for the study of periodically modulated weight kernels of the form $w(x; y) = \rho(|x - y|)\eta(y = \epsilon)$, we seek to describe the properties of fronts in terms of the behavior at the interface which separates high activity from low. If the front is not pulsating (which is the case in the absence of period modulation) then in a travelling wave frame (of the same speed as the wave) the rising edge of the front may be identified with a single (travelling wave) co-ordinate. For a pulsating front this point is no longer stationary in time and instead oscillates. We now show how to derive the dynamics for this *interface* between high and low activity states.
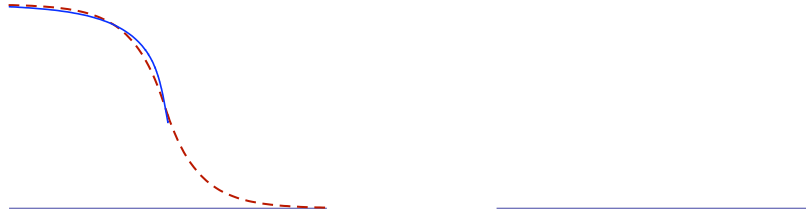
Figure 3. Wave fronts (solid lines) in the co-moving frame for $c = 0.1$ (left) and $c = 2$ (right), with $= 0.9$. Dashed curves are the fronts in the homogeneous model for the same wave speeds.

In a co-moving frame the model (1) takes the form $u = u(\;; t)$ where $= x \quad c_0 t$ for some fixed c_0 and

$$c_0 u + u_t = u + \;; \tag{17}$$

where

$$(\;; t) = \int_1^1 dy\, w(\; + c_0 t; y)\, f(u(y \quad c_0 t; t)); \tag{18}$$

We define a moving interface (level set) according to

$$u(\;_0(t); t) = h; \tag{19}$$

for some constant h. Here we are assuming that there is only one point on the interface (though in principle we could consider a set of points). Differentiation of (19) gives an exact expression for the velocity of the interface in the form

$$-_0 = \left. \frac{u_t}{u} \right|_{= _0(t)} : \tag{20}$$

Focusing now on the case of a Heaviside firing rate with $f(u) = H(u \quad h)$ means that for a pulsating front solution with $u > h$ for $<_0$ (18) takes the simple form

$$(\;; t) = \int_1^{_0 + c_0 t} dy\, w(\; + c_0 t; y); \tag{21}$$

3.1. **Perturbation analysis.** We now consider the case of small and expand $w(x; y)$ using (6), as

$$w(x; y) \; (x \quad y)[1 + (jx \quad yj \quad 1) \sin(2 \; y=\;)]; \tag{22}$$

For $= 0$ there is a travelling front $q(\;)$ given by the solution of

$$c_0 \frac{dq}{d} = q + \;; \qquad (\;) = \int_1^1 dy\; (y); \tag{23}$$

where the speed c_0 is determined by $q(0) = h$. For small we assume that the slope of the travelling front varies sufficiently slowly so that we may make the convenient approximation $u_j|_{= _0(t)} = q_j|j$

and (23), that

$$u_t|_{\xi = \xi_0(t)} = \int_{-1}^{\xi_0 + c_0 t} dy\, w(\xi_0 + c_0 t; y) \int_0^{1} dy'\, \eta(y'); \tag{24}$$

$$u_\xi|_{\xi = \xi_0(t)} = \frac{1}{c_0} h \int_0^{1} dy'\, \eta(y') : \tag{25}$$

Substitution of equations (24) and (25) into equation (20) gives

$$\dot{\xi}_0 = c_0 \frac{\int_0^{1} dy'\, \eta(y')(|y| - 1)\sin(2\pi(\xi_0 + c_0 t - y') = \epsilon)}{h \int_0^{1} dy'\, \eta(y')} : \tag{26}$$

Performing the integrals in (26) we find that the time-dependent speed of the front is given by $c_0(1 + \epsilon a(\xi_0; t))$ where $c_0 = (1 - 2h)=(2h)$ and

$$a(\xi_0; t) = A \sin\left[\frac{2\pi}{\epsilon}(\xi_0 + c_0 t) - \phi\right]; \tag{27}$$

with

$$A = \frac{1}{1 - 2h}\frac{2\pi=\epsilon}{1 + (2\pi=\epsilon)^2}; \qquad \tan\phi = -\frac{(2\pi=\epsilon)^2 - 1}{(2\pi=\epsilon)^2}: \tag{28}$$

Pulsating fronts are T-periodic solutions of the non-autonomous ordinary differential equation (26) with $\xi_0(t) = \xi_0(t + T)$. Introducing $x_0 = \xi_0 + c_0 t$ with $x_0 \in [0; \epsilon]$ we may solve for the trajectory using

$$\int_0^{x_0} \frac{dx}{1 + \epsilon A \sin(2\pi x=\epsilon - \phi)} = c_0 t: \tag{29}$$

Using a half angle substitution we may evaluate this to give

$$c_0 t = -\frac{1}{a}\tan^{-1}\left[\frac{\epsilon}{a}\frac{z_0(t) + \epsilon A}{z_0(0) + \epsilon A}\right]; \qquad a^2 = 1 - \epsilon^2 A^2; \tag{30}$$

where $z_0(t) = \tan[(2\pi x_0(t)=\epsilon - \phi)=2]$ and $x_0(0) = 0$. A periodic pulsating front with speed $c = \epsilon=T$ can be found by demanding that $\epsilon = x_0(T)$. Substitution of this condition into (30) shows that the speed of the pulsating front is given by

$$c = c_0\sqrt{1 - \epsilon^2 A^2}: \tag{31}$$
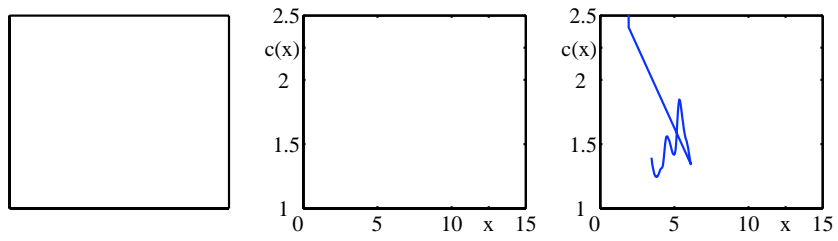
Hence, a propagating wave is only supponed [gh sp3

Figure 6. Left: Fluctuating ring threshold $h(x)$ for $\overline{h} = 0{:}2$, $a = 1$ and $= 0{:}2$. Middle: $c(x) = (1 \quad 2h(x))=(2h(x))$. Right:

Figure 7. Destabilisation of a spot in a 2D model with Mexican hat connectivity (as used in [16] with = 0.5 and = 4) and spatio-temporal fluctuations of the firing threshold ($\overline{h}$ = 0.05, a = 0.1, = 0.5 and = 1). From top left to bottom right: plots of $u(\mathbf{r}; t)$ at $t = 0$, $t = 25$, $t = 50$, $t = 100$, $t = 150$ and $t = 200$. Simulations were done with a simple Euler scheme and the use of 2D Fast Fourier transforms to compute convolutions, with a spatio-temporal discretisation $x = 0.05$ and $t = 0.1$ on a spatial grid of size 1536 1536.
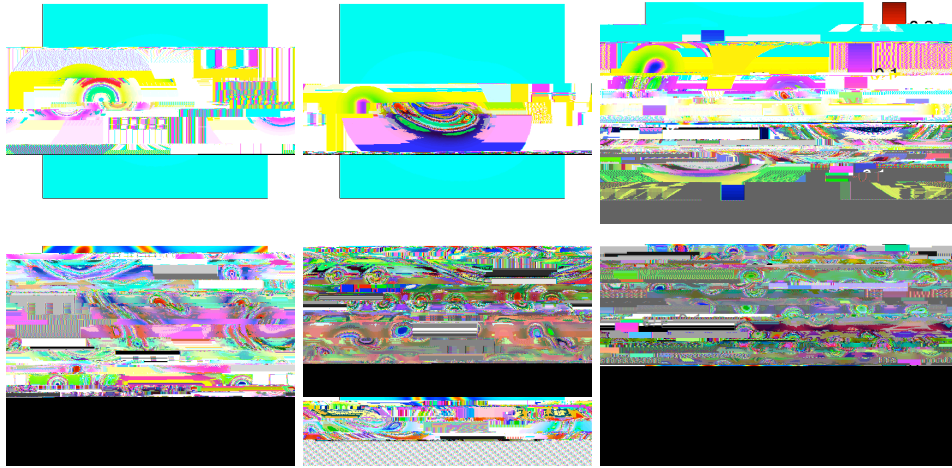

Figure 8. Destabilisation of a spot in a 2D model with Mexican hat connectivity (as used in [16] with = 0.5 and = 4) with spatial fluctuations of the firing threshold ($\overline{h}$ = 0.05, a = 0.1 and = 0.5) and adaptation with g = 0.1. From top left to bottom right: plots of $u(\mathbf{r}; t)$ at $t = 0$, $t = 50$, $t = 100$, $t = 200$, $t = 400$ and $t = 800$. The numerical scheme is the same as that used for Fig. 7 with $t = 0.02$.
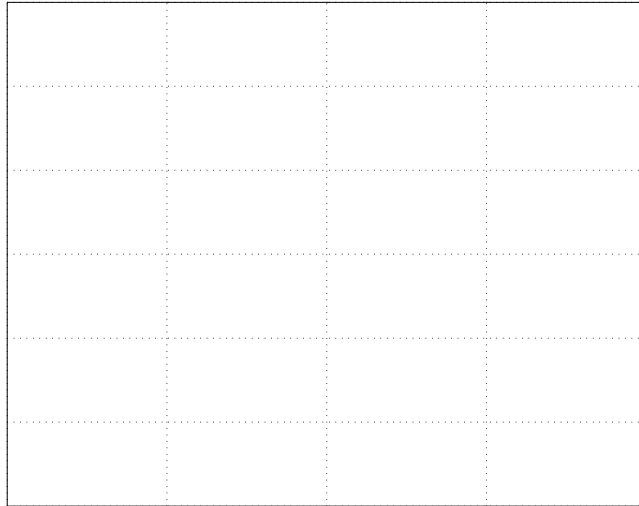
Figure 10. Speed of a bump of activity as a function of ring rate threshold h. Solid line: $=20$. Dashed line: is spatial white noise (see text for details). Upper branches are stable, lower unstable. Other parameters: $=15$ and $B=0.4$.

where $b(x)$ is a *template* function [19], chosen to be $\cos(x)$ in this case. Equation (47) is the result of minimising the L^2 norm between u and b [20, 21]. After suitably discretising eqns. (45)-(47) in space, solutions of the resulting system can be followed as parameters are varied, using (for example) pseudo-arclength continuation. An example of the results obtained is shown in Fig. 10 (solid line) where we plot c as a function of h for $=20$. We see that a stable and unstable bump are destroyed in a saddle-node bifurcation as h is increased.

The form of (45)-(47) suggests that one could introduce spatial heterogeneity to them, average over many realisations of this heterogeneity, and then solve the resulting equations in order to determine the e ects of this heterogeneity. As an example, consider (the gain of the ring rate function f) to be spatial white noise. In practice, this means that at each of the 1000 spatial points used in the calculation of the term $\int_0^2 dy$ in *realisations of this heterogeneity, and*

templ]TJ/F76.9471(,28(hose1817.)621(n)39Td227f3.616Td[(norm)24611949.9626T-5066940Td[)44.696Td[)443
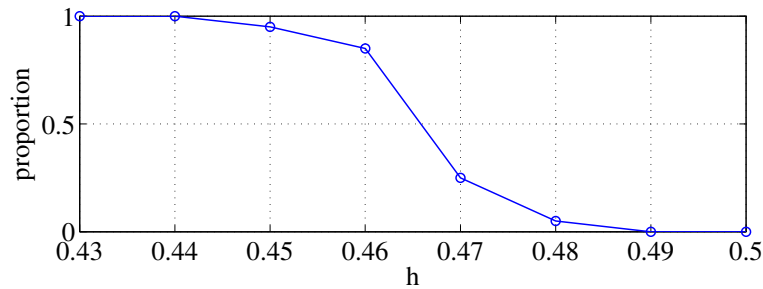*noi266-4446)TJ/F439.9626Tf28.8010T5and R.3F8w432.m56.314andISQease. EquB*

Figure 11. Proportion of simulations showing successful propagation of a bump as a function of h. Other parameters: $B = 0.4$.

where the angled brackets indicate averaging over i and

$$f[u; \beta] = \frac{1}{1 + e^{-\beta(u-h)}},\qquad(51)$$

will give information about the behaviour of (40)-(41) for a typical realisation of the $\alpha^i(x)$. The results of solving (48)-(50) when $m = \beta = 20$ are shown in Fig. 10 (dashed line). (We average over 2500 realisations of the $\alpha^i(x)$. Increasing this number, or increasing the number of spatial points used to calculate the integral $\int_0^{R_2} dy\, G(\alpha - y)f(u(y))$ does not qualitatively change the results presented.) From Fig. 10 we see that including such heterogeneity should (i) lower the maximum value of h for which a moving bump exists, and (ii) slightly decrease the speed of a stable moving bump. To illustrate that the first effect occurs we plot in Fig. 11, for several values of h, the proportion of 20 simulations for which a moving bump propagates, where (for fixed h) each of the 20 simulations uses a different realisation of $\alpha(x)$. We see the gradual failure of propagation and, for example, that at $h = 0.49$ none of the simulations showed a propagating bump, whereas from Fig. 10, if α was constant over space, a stable bump would propagate at this parameter value. We also observed numerically that such spatial disorder does slightly decrease the stable bump's speed (not shown).

4.3. **Neural field models driven by temporal noise.** Another method for incorporating randomness in a neural field model is to drive it with spatio-temporal noise. For simplicity we focus here on purely temporal noise; we will use some of the ideas presented in [Tf 6.642 -2.463 Td [(2)]Tr s-353(to)-lg.
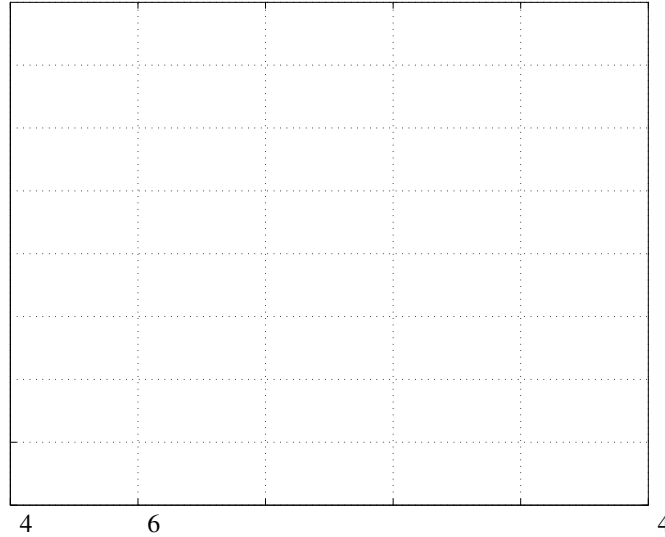
4   6   4

Figure 12. Speed of a moving bump solution of (54)-(55) for
(from top to bottom) $D = 0$, 0.001 and 0.003. At each value of
B, 5 simulations of duration 1000 time units were performed and
the mean speed for each simulation was measured. The mean and
standard deviation of these 5 speeds are plotted. Other parameters:
$= 5$, $h = 0.4$, $= 20$ and $= 1$.

$h \ (t)i = 0$ and $h \ (t) \ (s)i = D \ \exp \ (\ jt \ sj)$. D is the noise intensity and $1= \ $ is
the correlation time of the noise. Moving to a coordinate frame travelling at speed
$c(t)$, (52)-(53) become

$$u_t(\ ;t) = c(t)u \ (\ ;t) \ u(\ ;t) + \int_0^2 dyG(\ y)f(u(y;t)) \ a(\ ;t) + \ (t); \quad (54)$$

$$a_t(\ ;t) = c(t)a \ (\ ;t) + \frac{Bf(u(\ ;t)) \ a(\ ;t)}{} : \quad (55)$$

Although we can no longer nd xed points of (54)-(55) because of the presence of
the noise term (t), we can still *freeze* solutions using (for example) (47) and simu-
late (54)-(55) with (

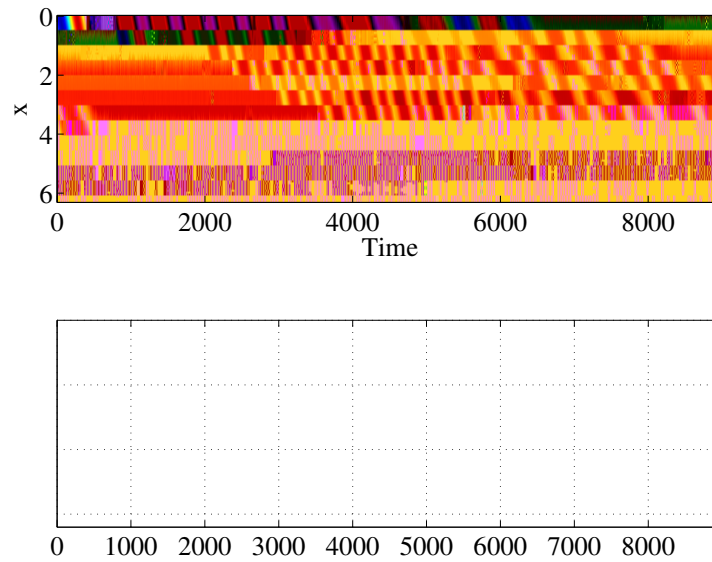Figure 13. Top: simulation of (52)-(53) with additive noise and $B = 0.07$ for $D = 0$ $(0 < t < 3000)$, $D = 0.001$ $(3000 < t < 6000)$ and $D = 0.003$ $(t > 6000)$. $u(x, t)$ is shown colour-coded. Bottom: instantaneous bump speed extracted from the simulation in the top panel. Other parameters: $= 5$, $h = 0.4$, $= 20$ and $= 1$.

bifurcation (i.e. only moving bumps are stable) whereas for $D = 0.003$, $B = 0.07$ is to the left of the bifurcation, and the only stable state is a stationary bump.

5. **Discussion.** It is hard even at a first approximation to view the brain as a homogeneous system and so there is a pressing need to develop a set of mathematical tools for the study of waves in heterogeneous media that can be used in brain modelling. Homogenization is one natural multi-scale approach that can be utilised in this regard, and we have revisited the mathematical foundations of this approach in the context of non-local integral models that arise in neural field modelling. As a perturbation technique it requires that modulation on the micro-scale be both small in amplitude and rapidly varying in space, and as such is limited in its range of applicability. For the special case of a Heaviside firing rate function we have shown how improved results can be obtained (circumventing the need for rapid spatial

informative to adapt recent ideas developed for the numerical study of waves in stochastic PDEs [21]. In this sense it is likely that other ideas from applied dynamical systems [27] may be usefully adapted for the study of non-local random neural systems.

We have focused mainly on developing results in one spatial dimension and it remains to perform the extension to two spatial dimensions. Although both homogenization and interface formalisms go over naturally to two spatial dimensions the solution of the resulting models will no doubt remain a challenge | if nothing else but for the reason that solutions in 2D can come in a variety of rich forms such as spiral waves, labyrinthine structures and replicating and rotating collections of bumps [28, 16]. A generalisation of the freezing approach discussed in Secs. 4.2-4.3 has been applied to spiral waves in reaction-diffusion systems [20, 29] and it should be possible to apply them to waves in 2D neural field models. The development of a 2D interface dynamics for translation invariant kernels is currently under development and is likewise expected to form the basis for a perturbation theory for modulated connectivities. These and related ideas will be presented elsewhere.

Appendix A. Here we give an outline of the derivation of the homogenized version of (1) by means of two-scale convergence techniques. The detailed derivation of (4) will be presented in a complementary paper [30]. We write the original model in the form

$$\frac{\partial}{\partial t}u_\eta(x;t) = -u_\eta(x;t) + \int_{-1}^{1} w_\eta(x';x;\frac{x'}{\eta})f(u_\eta(x';t))\mathrm{d}x'; \qquad (56)$$

where $w_\eta(x;y) = (|x|;\omega(y))\Omega(y)$. The relationship between w_η and w is given by $w(x;y) = w_\eta(x-y;y=\eta)$. It turns out that this formulation of a neural field model is tractable when using two scale convergence techniques.

We view (56) as a one-parameter family of neural field models, parametrized by η. The initial value problem of (56) is, according to Potthast *et al.* [31], globally well-posed in the Banach space of bounded, continuous functions for connectivity functions which are uniformly bounded in both the supremum norm and the L^1-norm and satisfy a Hölder condition, and firing rate functions which take values between 0 and 1. One notable property is that the η-dependent solution is uniformly bounded, where the bound depends on the supremum norm of the initial condition and the bounding constant of the connectivity function in the L^1-norm. We assume from now on that the conditions prescribed in Potthast *et al.* [31] are fulfilled.

For our purposes we will need the existence and boundedness of solution u_η in $L^2(\mathbb{R})$. From Theorem 3.2.1 in Faye *et al.* [32], which is a straightforward adaptation of a classical result by Hale *et al.* [33] for first order functional differential equations, we get the following result:

Lemma 1. Assume that $w \in L^2(\mathbb{R})$ and that the initial condition $u_\eta(x;0) = U(x)$ is square integrable, i.e. $U \in L^2(\mathbb{R})$. Then there is a unique solution $u_\eta \in L^2([0;T];L^2(\mathbb{R}))$ of (56) which obeys the uniform bounds

$$\|u_\eta\|_{L^1([0;T];L^2(\mathbb{R}))} \le C_1 \left(\|U\|_{L^2(\mathbb{R})} + \|w\|_{L^2(\mathbb{R})} \right); \qquad (57)$$

and

$$\|u_\eta\|_{L^2([0;T];L^2(\mathbb{R}))} \le C_1 \left(\|U\|_{L^2(\mathbb{R})} + \|w\|_{L^2(\mathbb{R})} \right): \qquad (58)$$

for some constants $C_1 > 0$ and $T > 0$.

Just as in [34, 35] we get the following results:

Lemma 2. Let the initial condition $u_\varepsilon(x, 0) = U(x)$ of (56) belong to the intersection $L^1(\mathbb{R}) \setminus L^1(\mathbb{R})$ and assume that

$$\sup_{x \in \mathbb{R}} \int_{-1}^{1} w_\varepsilon(x, y) dy \leq C$$

for some positive constant $C > 0$. Then there exists a unique $u_\varepsilon \in C(\mathbb{R}_0^+; L^1(\mathbb{R}) \setminus L^1(\mathbb{R}))$ satisfying (56). Moreover, we have the uniform bounds

$$\max_{0 \leq t \leq T} \| u_\varepsilon \|_{L^1(\mathbb{R})} \leq C \| U \|_{L^1(\mathbb{R})}$$

and

$$\max_{0 \leq t \leq T} \| u_\varepsilon \|_{L^1(\mathbb{R})} \leq C \| U \|_{L^1(\mathbb{R})}$$

for some $T > 0$.

The proofs of Lemma 1 and Lemma 2 will be presented in a forthcoming paper [30].

Next, let us define the concept of two-scale convergence: Let $\mathbb{T}$ denote the 1-dimensional unit torus (or unit circle) and let $Y = [0, 1]$. We identify the Y-periodic functions by those functions that are defined on $\mathbb{T}$ and introduce functions $\varphi \in L^2(\mathbb{R} \times \mathbb{T})$ and consider their traces $\varphi(x, x = \varepsilon)$. Assume that $\{v_\varepsilon\}$ is a bounded sequence in $L^2(\mathbb{R})$. The sequence $\{v_\varepsilon\}$ is said to *two-scale converge* to v

Now, according to Remark 7 in [36] it is possible to modify the definition of two-scale convergence in L^2-spaces to obtain a definition of two-scale convergence in L^1-spaces; see also [37]. The test functions are chosen here to be continuous with compact support in x and continuous and Y-periodic in y. It is crucial that we can include the L^1-case since it turns out in the application of two-scale convergence to the convolution integral in (1) that one of the terms is assumed to two-scale converge in L^1. So the fundamental question now is how to determine the limit of the convolution term as $\varepsilon \to 0$. The following theorem which originally was proved by Visintin [37] gives the answer to that question:

Theorem 1. Suppose that $\{v_\varepsilon\}$ is a sequence of two-scale functions converging to $v \in L^2(\mathbb{R}; L^2(\mathbb{T}))$ and that $\{w_\varepsilon\}$ is two-scale converging to $w \in L^1(\mathbb{R}; L^1(\mathbb{T}))$. Then the convolution integral

$$[w_\varepsilon * v_\varepsilon](x) \qquad Z_1$$

[7] B W Connors and Y Amitai. Generation of epileptiform discharges by local circuits in neo-cortex. In P A Schwartzkroin, editor, *Epilepsy: Models, Mechanisms and Concepts*, pages 388{424. Cambridge University Press, 1993.

[8] O Faugeras, F Grimbert, and J-J Slotine. Absolute stability and complete synchronization in a class of neural elds models. *SIAM Journal on Applied Mathematics*, 69:205{250, 2008.

[9] P C Bresslo . Traveling fronts and wave propagation failure in an inhomogeneous neural network. *Physica D*, 155:83{100, 2001.

[10] H Schmidt, A Hutt, and L Schimansky-Geier. Wave fronts in inhomogeneous neural eld models. *Physica D*, 238:1101{1112, 2009.

[11] S Coombes and C R Laing. Pulsating fronts in periodically modulated neural eld models. *Physical Review E*, 83:011912, 2011.

[12] C A Brackley and M S Turner. Persistent uctuations of activity in undriven continuum neural eld modles with power-law connections. *Physical Review E*, 79:011918, 2009.

[13] C A Brackley and M S Turner. Random uctuations of the ring rate function in a continuum neural eld model. *Physical Review E*, 75:041913, 2007.

[14] J Keener. Homogenization and propagation in the bistable equation. *Physica D*, 136:1{17, 2000.

[15] G Nguetseng. A general convergence result of a functional related to the theory of homoge-nization. *SIAM Journal on Mathematical Analysis*, 20:608{623, 1989.

[16] M R Owen, C R Laing, and S Coombes. Bumps and rings in a two-dimensional neural eld: splitting and rotational instabilities. *New Journal of Physics*, 9:378, 2007.

[17]